Journal of Fluids and Structures (2002) **16**(7), 931–955
doi:10.1006/jfls.454 available online at http://www.idealibrary.com on IDEAL®

AEROELASTIC MODEL OF VOCAL-FOLD-SHAPED VIBRATING ELEMENT FOR STUDYING THE PHONATION THRESHOLD

J. Horáček

Institute of Thermomechanics, Academy of Sciences of the Czech Republic
Dolejškova 5, 182 00 Prague 8, Czech Republic

AND

J. G. Švec
Medical Healthcom, Ltd., Centre for Communication Disorders, Řešovská 10/491
181 00 Prague 8, Czech Republic
and
W. J. Gould Voice Center, the Denver Center for the Performing Arts, 1245 Champa Street
Denver, CO 80206, U.S.A.

(Received 20 March 2001; and in final form 15 February 2002)

An original theoretical model for vibration onset of the vocal folds in the air-flow coming from the human subglottal tract is designed, which allows studying the influence of the physical properties of the vocal folds (e.g., geometrical shape, mass, viscosity) on their vibration characteristics (such as the natural frequencies, mode shapes of vibration and the thresholds of instability). The mathematical model of the vocal fold is designed as a simplified dynamic system of two degrees of freedom (rotation and translation) vibrating on an elastic foundation in the wall of a channel conveying air. An approximate unsteady one-dimensional flow theory for the inviscid incompressible fluid is presented for the phonatory air-flow. A generally defined shape of the vocal-fold surface is considered for expressing the unsteady aerodynamic forces in the glottis. The parameters of the mechanical part of the model, i.e., the mass, stiffness and damping matrices, are related to the geometry and material density of the vocal folds as well as to the fundamental natural frequency and damping known from experiments. The coupled numerical solution yields the vibration characteristics (natural frequencies, damping and mode shapes of vibration), including the instability thresholds of the aeroelastic system. The vibration characteristics obtained from the coupled numerical solution of the system appear to be in reasonable qualitative agreement with the physiological data and clinical observations. The model is particularly suitable for studying the phonation threshold, i.e., the onset of vibration of the vocal folds.

1. INTRODUCTION

The understanding of the biomechanics of human voice production has increased substantially during last few years [see, e.g., Titze (1994)]. Human voice normally originates in the larynx. When air passes the space between the vibrating vocal folds called

0889-9746/02/070931 + 25 $35.00/0

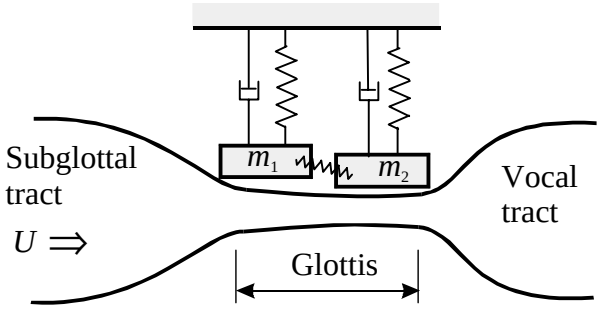

Figure 1. Scheme of the coupled two-mass model of the vocal folds (Ishizaka & Flanagan 1972).

glottis, the vibration of the vocal folds is excited as a result of a fluid–structure interaction mechanism. The glottal oscillations serve as the main generator of the acoustic excitation of the whole human vocal tract, which finally results in phonation.

Even if the vocal folds are living soft tissues of a complicated material structure composed of several tissue layers, and their motion is generally a 3-D motion of a continuous viscoelastic system, they are frequently modelled as dynamic systems with only a few degrees of freedom (Titze 1994).

The simplest model is a one-mass model where a simple harmonic oscillator represents each vocal fold (Flanagan & Landgraf 1968). More frequently, two-mass models coupled by stiffness are used for each vocal fold. Figure 1 depicts the original two-mass model developed by Ishizaka & Flanagan (1972), that provides the basis for the two-degree-of-freedom models that have been most frequently used for simulation of voice and speech. In the last decade, the Ishizaka and Flanagan model was modified, e.g. by Pelorson *et al.* (1994*a*,*b*) or Steinecke & Herzel (1995). The two-mass models make it possible to simulate a phase delay between the inlet and outlet parts of the glottis, which has been considered an important feature observed in real vocal folds [see, e.g., Titze (1994)]. A slightly different two-degree-of-freedom model of the vocal folds, the simplified translating and rotating mass model, was developed by Liljencrants (1991). This model of two coupled mechanical resonators is similar to the model presented here.

Aerodynamic forces, which excite such systems, can be modelled by more or less complicated expressions for the pressure P in the glottis derived on the basis of the Bernoulli energy law, e.g., in the following form:

$$P = (1 - a_2/a_1)\,(P_s - P_i) + P_i.$$

where a_1 is the cross-sectional area of the glottis at the entry (inlet), a_2 is the cross-sectional area of the glottis at glottal exit (outlet), P_s is the subglottal pressure and P_i is the pressure at the outlet of glottis (Titze 1994). Similar expressions for the aerodynamic forces developed on the basis of the so-called myoelastic-aerodynamic theory of vocal-fold vibration can be found in papers where the motion of the vocal folds is simulated (Mergell 1998; Reuter *et al.* 1999). However, the coupling between the flowing air and the mechanical system is given here only by the cross-sections $a_1(t)$ and $a_2(t)$, which are dependent on the displacements of the masses. Any influence of the shape of the vocal folds on the aerodynamic excitation forces is not included.

Pelorson *et al.* (1994*a*, *b*) have incorporated a more realistic rounded shape of the vocal folds into the Ishizaka–Flanagan model and have also included the consideration of a moving fluid separation point, on the basis of their experiments on the characteristics of jet flows in simulated diverging glottal shapes (Pelorson *et al.* 1995). The glottal geometry

considered there, however, did not include a factor such as the bulging shape of the vocal folds [e.g., Alipour & Scherer (2000)], which influences the resulting aerodynamic forces acting on the focal folds. Here, we present an approach that, among others, enables taking the bulged shape of the vocal folds into account. The shape of the vocal fold according to Berry *et al.* (1994) is considered, in which a smooth convergent glottal inlet changes into a very short diverging part. There is a sharp-edged outlet, at which the flow separates, forming a free jet.

Recently, Lous *et al.* (1998) theoretically analysed a more complex model of voice production, which included also the influence of acoustic properties of subglottal and supraglottal systems on the glottal flux during phonation. The original asymmetric distribution of the two masses and stiffnesses in each of the vocal folds (Ishizaka & Flanagan 1972) was replaced by a symmetrical one, which allowed for considerable simplifications of the equations of the two-mass model of the vocal folds. The aerodynamic forces calculated from the Bernoulli equation were assumed to act on three massless plates, which determined a piecewise linear shape of each vocal fold. For a basic model a quasistationary incompressible frictionless fluid flow was supposed, and the time-dependent lung pressure $p_0(t)$ drove the phonation. However, there is no clear relationship between the parameters of the mechanical model and the characteristics of the real vocal folds. De Vries *et al.* (1999) published a sophisticated method for relating the parameters of the Ishizaka–Flanagan and Pelorson mechanical models to the more advanced, high-dimensional finite element models of the vocal folds. In the approach presented here, we attempt to directly relate the properties of the vocal-fold model to the characteristics measured on the real vocal folds.

Lucero (1999) theoretically studied the nonlinear phenomena (Hopf bifurcations) when the equilibrium position of the vocal folds becomes unstable. The thresholds of the stability are given by a critical value of the subglottal pressure or by a critical value of the glottal half-width. The nonlinear effects are caused by a motion of the flow separation point during oscillations, when big changes of the shape of the glottis are considered. The vocal-fold model is different from the model presented here, because Lucero used a mucosal wave model described by a one-degree-of-freedom dynamic system.

The approach presented here takes into account small amplitudes of the vocal folds and focuses on the threshold states of the vocal-fold oscillation. Numerical solution of the coupled fluid-structural vibrations is offered which enables to study frequency modal characteristics (natural frequencies, damping and mode shapes of vibration) and instability thresholds of the aeroelastic system. A linear two-degree-of-freedom mechanical system with simultaneous mass and stiffness coupling is used for modelling the vocal-fold vibration (Figure 2). This system is equivalent to the dynamical system which consists of three joined masses vibrating on an elastic continuous foundation (Figure 3). Parameters of the mechanical part of the model, i.e., the mass, stiffness and damping matrices, are approximately related to the physiological data, because they are given by a real geometry of the vocal folds, by the tissue density, and by the fundamental natural frequency and damping known from experiments. It can be noted that, despite of the attempts starting already with Ishizaka & Flanagan (1972), there is often not such a direct relationship between real data and the values of lumped parameters of the simplified models. The unsteady aerodynamic forces are calculated using one-dimensional flow theory for inviscid incompressible fluid in the glottis, where the geometrical profile of the vocal folds is modelled. A potential flow in the glottis is considered up to the point of flow separation, which is assumed at the sharp trailing edge of the vocal-fold-shaped element corresponding to a converging prephonatory shape of the glottis (see Figure 4). Considering small vibration amplitudes up to only the threshold state makes it possible

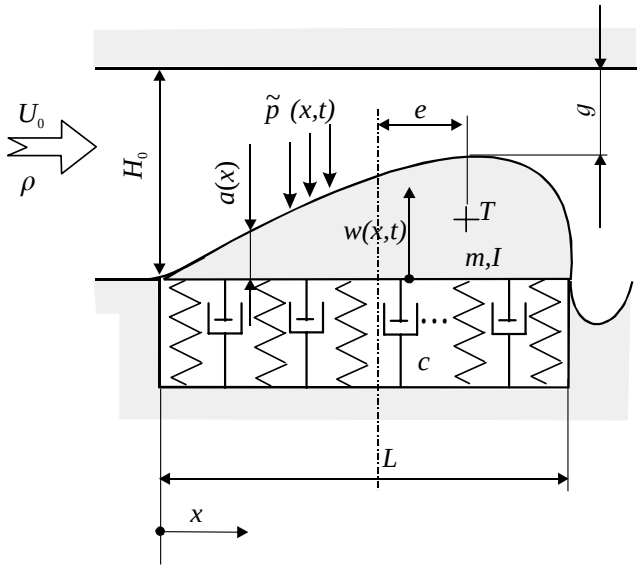

Figure 2. Two-degree-of-freedom model of the vocal folds in the air-flow through the glottis.

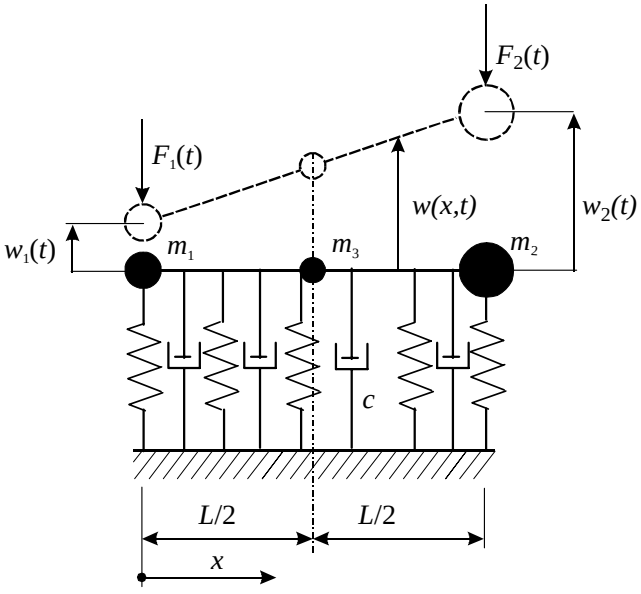

Figure 3. Schematic of the equivalent mechanical system.

to disregard the motion of the flow separation point, which takes place only in relatively large oscillatory amplitudes at flow-divergent glottal configuration shapes. In the model presented here it is supposed that the phonation is driven by a self-oscillation mechanism after crossing a threshold of control parameters for the occurrence of instability in the system.

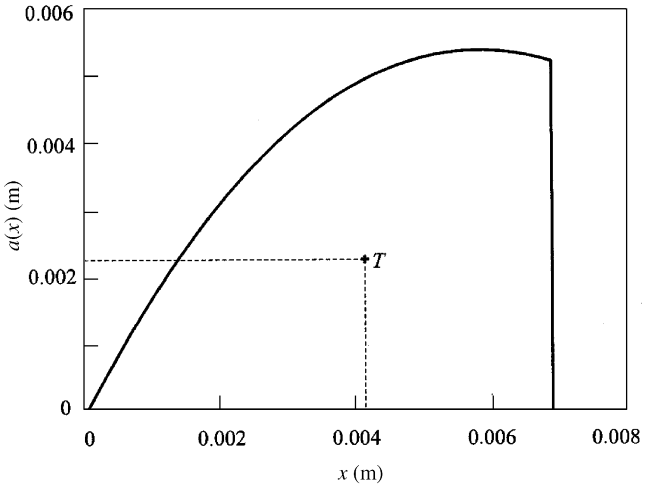

Figure 4. Geometry of the vocal fold considered with the centre of gravity at T.

A similar theoretical model was developed by the authors for a flexibly supported uniform flat plate vibrating in the wall of a 2-D channel conveying fluid (Simerská & Horáček 1996; Horáček *et al.* 1997). Here, the theory is refined by considering a general profile of the vibrating body, and modified by assuming a continuous elastic foundation instead of discrete springs underneath.

First, the equations of motion describing the vibration of the vocal-fold-shaped element will be presented here. Second, the unsteady aerodynamic forces will be ascertained and the theoretical solution will be presented for calculation of the frequency/modal characteristics and stability boundaries of the system under investigation. Then several numerical examples will be given for real data published in the literature, and the results will be qualitatively compared with the experiments and clinical observations of real human vocal-folds behaviour.

2. EQUATIONS OF MOTION

Symmetric oscillations of the vocal folds are assumed, and thus only half of the glottal region is modelled here. The studied fluid–elastic system is schematically shown in Figure 2, and a simplified scheme of the mechanical part is presented in Figure 3. The equations of motion are derived in detail in Appendix A.

The vibrating body of the mass m, with the moment of inertia I and the centre of gravity T at the location e is replaced by an equivalent three-mass system, where the masses

$$m_{1,2} = \frac{2}{L^2}\left(I + me^2 \mp me\frac{L}{2}\right), \quad m_3 = m\left[1 - 4\left(\frac{e}{L}\right)^2\right] - \frac{4}{L^2}I \tag{1}$$

are joined together by a solid massless rod of length L; $w_{1,2}(t)$ are the displacements of masses $m_{1,2}$; c is the stiffness of the elastic foundation per unit length. The masses $m_{1,2}$ are located at the ends of the rod and the mass m_3 is in the middle (see Figure 3). The function $a(x)$ in Figure 2 defines the aerodynamic shape of the body oscillating in a channel

containing fluid of the density ρ which enters the glottal region with mean flow velocity U_0 at the inlet ($x = 0$), where H_0 is the height of the channel. The perturbation aerodynamic pressure $\tilde{p}(x, t)$ is caused by the deflection $w(x, t)$ of the body:

$$w(x, t) = (x - L/2)V_1(t) + V_2(t), \tag{2}$$

where the quantities

$$V_1(t) = [w_2(t) - w_1(t)]/L, \quad V_2(t) = [w_2(t) + w_1(t)]/2 \tag{3}$$

represent the pitch and heave motions of the body, or the modes $\times 10$ and $\times 11$ (Titze 1994; Berry *et al.* 1994). The equivalent aerodynamic excitation forces (Figure 3) are given by the integrals

$$F_1(t) = h \int_0^L \tilde{p}(x, t)(1 - x/L)\,\mathrm{d}x, \quad F_2(t) = h \int_0^L \tilde{p}(x, t)(x/L)\,\mathrm{d}x. \tag{4}$$

where h is the width of the channel; t is the time and x is the axial coordinate.

According to Appendix A, the equations of motion can be written as follows:

$$\mathbf{M}\ddot{\mathbf{V}} + \mathbf{B}\dot{\mathbf{V}} + \mathbf{K}\mathbf{V} + \mathbf{F} = \mathbf{0}, \tag{5}$$

where $\mathbf{M}$ and $\mathbf{K}$ are mass and stiffness matrices

$$\mathbf{M} = \begin{bmatrix} -m_1 L/2 & m_1 + m_3/2 \\ m_2 L/2 & m_2 + m_3/2 \end{bmatrix}, \quad \mathbf{K} = \begin{bmatrix} -kL/12 & k/2 \\ kL/12 & k/2 \end{bmatrix}. \tag{6}$$

A proportional damping matrix $\mathbf{B}$ [see, e.g., Inman (1989)] can be defined as follows:

$$\mathbf{B} = \varepsilon_1 \mathbf{M} + \varepsilon_2 \mathbf{K}, \tag{7}$$

where ε_1 and ε_2 are real constants, which can be approximately adjusted according to the experimental data (see Section 5.1. and Appendix C). The vectors

$$\mathbf{V}^T = [V_1(t), \quad V_2(t)], \quad \mathbf{F}^T = [F_1(t), \quad F_2(t)] \tag{8}$$

are the dynamic response and force vectors; $k = cL$ (N/m) is the coefficient of stiffness of the elastic foundation under the body; $(\,)^T$ denotes the transpose, and the overdot the time derivative.

The two-degree-of-freedom dynamic system presented reflects the fundamental translational and rotational motions of human vocal folds. These motions are crucially important for normal self-sustained oscillation of the vocal folds (Titze 1994). For example, considerably less important for phonation is the motion of the vocal folds in the air-flow (x) direction because the glottal gap is not changed by this motion. Berry & Titze (1996) considered a continuum model of the vocal folds vibrating *in vacuo* and calculated several of the lower natural mode shapes of vibration. The vibrations for the first mode were predominantly in the x-direction, while the second and third modes correspond to the translation and rotation, respectively, in the two-degree-of-freedom model presented here.

3. AERODYNAMIC FORCES

The one-dimensional (1-D) model of the unsteady fluid flow in the rectangular channel of the height $H(x, t)$ and the width h= const. is given by the following Euler (momentum) and

continuity equations [see, e.g., Norton (1989)]:

$$\rho \frac{\partial U(x,t)}{\partial t} + \rho U(x,t) \frac{\partial U(x,t)}{\partial x} + \frac{\partial P(x,t)}{\partial x} = 0, \tag{9}$$

$$\frac{\partial(\rho h H(x,t)\Delta x)}{\partial t} = (\rho U(x,t) h H(x,t))_x - (\rho U(x,t) h H(x,t))_{x+\Delta x}, \tag{10}$$

where the flow velocity $U(x,t)$ and pressure $P(x,t)$ can be considered to be composed of the steady and perturbation parts as follows:

$$U(x,t) = \bar{U}_0(x) + \tilde{u}(x,t), \quad P(x,t) = P_0(x) + \tilde{p}(x,t); \tag{11}$$

and according to the previous section (Figure 2),

$$H(x,t) = H_0 - w(x,t) - a(x). \tag{12}$$

Substitution of expressions (11) into equation (9) yields

$$\frac{\partial \tilde{u}}{\partial t} + \frac{\partial(\tilde{u}\bar{U}_0)}{\partial x} + \tilde{u}\frac{\partial \tilde{u}}{\partial x} = -\frac{1}{\rho}\frac{\partial \tilde{p}}{\partial x}, \tag{13}$$

where the Bernoulli equation,

$$\tfrac{1}{2}\rho \bar{U}_0^2(x) + P_0(x) = \text{constant}, \tag{14}$$

was used.

In the present paper the attention is focused on the phonatory threshold states, for the purpose of which only small velocity perturbations ($\tilde{u}(\partial\tilde{u}/\partial x) \to 0$) can be considered. Introducing the potential $\Phi(x,t)$, such that

$$\tilde{u} = \frac{\partial \Phi}{\partial x}, \tag{15}$$

the perturbation (acoustic) pressure is given by the integration of equation (13) over x:

$$\tilde{p} = -\rho\left(\frac{\partial \Phi}{\partial t} + \bar{U}_0(x)\frac{\partial \Phi}{\partial x}\right). \tag{16}$$

Substitution of expressions (11) for $U(x,t)$ and (12) for $H(x,t)$ into equation (10) yields

$$\frac{\partial w}{\partial t} = -\frac{\partial(w\bar{U}_0(x))}{\partial x} + H_0\frac{\partial \tilde{u}}{\partial x} - \frac{\partial(\tilde{u}w)}{\partial x} - \frac{\partial(a(x)\tilde{u})}{\partial x}, \tag{17}$$

where the continuity equation

$$\bar{U}_0(x)(H_0 - a(x)) = \text{constant} \tag{18}$$

for the steady flow was used. Integration of equation (17) over x gives

$$\tilde{u}(x,t) = \frac{1}{(H_0 - a(x) - w(x,t))}\left[\frac{\partial}{\partial t}\int w(x,t)\,\mathrm{d}x + w(x,t)\,\bar{U}_0(x)\right]. \tag{19}$$

For the phonatory threshold states, only small displacements $w(x,t) \ll H_0$ can be assumed, and substituting w from equation (2) into (19) the derivative (15) of the potential becomes

$$\frac{\partial \Phi}{\partial x} = \frac{1}{H_0 - a(x)}\left\{\frac{x^2}{2}\dot{V}_1(t) + \left[\dot{V}_2(t) - \frac{L}{2}\dot{V}_1(t)\right]x + \dot{C}(t) + \left[\left(x - \frac{L}{2}\right)V_1(t) + V_2(t)\right]\bar{U}_0(x)\right\}, \tag{20}$$

where $C(t)$ is an unknown function of time. The integration gives the potential in the form

$$\Phi(x,t) = \dot{V}_1(t)I_1(x) + \dot{V}_2(t)I_2(x) + \dot{C}(t)I_3(x) + V_1(t)I_4(x) + V_2(t)I_5(x) + \bar{C}(t), \quad (21)$$

where $\bar{C}(t)$ is another unknown time function and $I_i(x)$ $(i = 1, \ldots, 5)$ are the integrals given in Appendix B.

Using equations (20) and (21) the perturbation pressure (16) can be written as

$$\begin{aligned}\tilde{p}(x,t) = &-\rho[\ddot{V}_1(t)I_1(x) + \ddot{V}_2(t)I_2(x) + \ddot{C}(t)I_3(x) + \dot{V}_1(t)g_1(x)\\ &+ \dot{V}_2(t)g_2(x) + \dot{\bar{C}}(t) + \dot{C}(t)g_3(x) + V_1(t)g_4(x) + V_2(t)g_5(x)],\end{aligned} \quad (22)$$

where $g_i(x)$ $(i = 1, 2, \ldots, 5)$ are functions given in Appendix B.

Finally, substituting $\tilde{p}$ in equations (4) the aerodynamic forces are given by

$$\begin{aligned}F_1(t) = &-\rho h[\ddot{V}_1(t)J_1 + \ddot{V}_2(t)J_2 + \dot{V}_1(t)J_3 + \dot{V}_2(t)J_4\\ &+ V_1(t)J_5 + V_2(t)J_6 + \ddot{C}(t)J_7 + \dot{C}(t)J_8 + \dot{\bar{C}}J_9],\end{aligned} \quad (23)$$

$$\begin{aligned}F_2(t) = &-\rho h[\ddot{V}_1(t)J_{10} + \ddot{V}_2(t)J_{11} + \dot{V}_1(t)J_{12} + \dot{V}_2(t)J_{13}\\ &+ V_1(t)J_{14} + V_2(t)J_{15} + \ddot{C}(t)J_{16} + \dot{C}(t)J_{17} + \dot{\bar{C}}J_{18}],\end{aligned} \quad (24)$$

where J_i $(i = 1, \ldots, 18)$ are the integrals given in Appendix B.

The functions $C(t)$ and $\bar{C}(t)$ have to be determined from the boundary conditions for the flow at the inlet $(x = 0)$ and outlet $(x = L)$, which can be approximated as follows:

$$\tilde{u} = \frac{\partial \Phi}{\partial x} = 0|_{x=0} \quad \text{and} \quad \tilde{p} = 0|_{x=L}. \quad (25)$$

Satisfying the first of equation (25) and using equation (20) it can easily be found that

$$\dot{C}(t) = V_1(t)(U_0 L/2) - V_2(t)U_0; \quad (26)$$

similarly the second of equation (25) by using equation (22) yields

$$\begin{aligned}\dot{\bar{C}}(t) = &-\ddot{V}_1(t)I_1(L) - \ddot{V}_2(t)I_2(L) - \dot{V}_1(t)[I_3(L)(U_0 L/2) + g_1(L)] + \dot{V}_2(t)[I_3(L)U_0 - g_2(L)]\\ &- V_1(t)\big[g_4(L) + g_3(L)(U_0 L/2)\big] - V_2(t)\big[g_5(L) - g_3(L)U_0\big],\end{aligned} \quad (27)$$

where the mean flow velocity $\bar{U}_0(x)$ at the inlet $(x = 0)$ is denoted by U_0 for simplicity.

Finally, substituting the functions $\dot{C}(t)$ and $\dot{\bar{C}}(t)$ into equations (23) and (24), the unsteady aerodynamic forces $F_1(t)$ and $F_2(t)$ are expressed as functions of the displacements $V_1(t)$ and $V_2(t)$. The aerodynamic coefficients J_i given by the integrals in Appendix B are functions of only mean (steady) flow velocity $\bar{U}_0(x)$ and do not depend on time.

Using the continuity equation (18), the mean (steady) flow velocity in the glottis $(x \in \langle 0, L\rangle)$ is as follows:

$$\bar{U}_0(x) = \frac{U_0}{[1 - a(x)/H_0]}, \quad (28)$$

where U_0 and H_0 are the flow velocity and the height of the channel, respectively, at the inlet $(x = 0)$ to the glottal region. The function $a(x)/H_0$ is given by the geometry of the vocal folds and larynx. The air-flow velocity U_0 (m/s) is simply related to the so-called glottal volume velocity (glottal flux)

$$Q = U_0 2H_0 h, \quad (29)$$

which represents one of the most important physiological characteristics of voiced sound production; for male adults it is normally in the range $Q = 0 - 0{\cdot}6$ l/s (Pelorson 1995).

4. SOLUTION OF THE COUPLED PROBLEM

Substitution of the aerodynamic forces $F_{1,2}(t)$ from the equations (23), (24), (26) and (27) in the equation of motion (5) gives

$$\mathbf{M}\ddot{\mathbf{V}} + \mathbf{B}\dot{\mathbf{V}} + \mathbf{K}\mathbf{V} - \rho h\{\hat{\mathbf{M}}\ddot{\mathbf{V}} + \hat{\mathbf{B}}\dot{\mathbf{V}} + \hat{\mathbf{K}}\mathbf{V}\} = \mathbf{0}, \tag{30}$$

where the mass, damping and stiffness matrices of unsteady aerodynamic origin are:

$$\hat{\mathbf{M}} = \begin{bmatrix} J_1 - J_9 I_1(L) & J_2 - J_9 I_2(L) \\ J_{10} - J_{18} I_1(L) & J_{11} - J_{18} I_2(L) \end{bmatrix}, \tag{31}$$

$$\hat{\mathbf{B}} = \begin{bmatrix} \hat{B}_{11} & \hat{B}_{12} \\ \hat{B}_{21} & \hat{B}_{22} \end{bmatrix}, \quad \hat{\mathbf{K}} = \begin{bmatrix} \hat{K}_{11} & \hat{K}_{12} \\ \hat{K}_{21} & \hat{K}_{22} \end{bmatrix}, \tag{32}$$

where

$$\begin{aligned} \hat{B}_{11} &= J_3 + J_7 U_0 \frac{L}{2} - J_9 \left[I_3(L) U_0 \frac{L}{2} + g_1(L) \right], \\ \hat{B}_{12} &= J_4 - J_7 U_0 + J_9 [I_3(L) U_0 - g_2(L)], \\ \hat{B}_{21} &= J_{12} + J_{16} U_0 \frac{L}{2} - J_{18} \left[I_3(L) U_0 \frac{L}{2} + g_1(L) \right], \\ \hat{B}_{22} &= J_{13} - J_{16} U_0 + J_{18} [I_3(L) U_0 - g_2(L)], \end{aligned} \tag{33}$$

and

$$\begin{aligned} \hat{K}_{11} &= J_5 + J_8 U_0 \frac{L}{2} - J_9 \left[g_4(L) + g_3(L) U_0 \frac{L}{2} \right], \\ \hat{K}_{12} &= J_6 - J_8 U_0 - J_9 [g_5(L) - g_3(L) U_0], \\ \hat{K}_{21} &= J_{14} + J_{17} U_0 \frac{L}{2} - J_{18} \left[g_4(L) + g_3(L) U_0 \frac{L}{2} \right], \\ \hat{K}_{22} &= J_{15} - J_{17} U_0 - J_{18} [g_5(L) - g_3(L) U_0]. \end{aligned} \tag{34}$$

Introducing the matrices

$$\mathbf{A} = \mathbf{M} - \rho h \hat{\mathbf{M}}, \tag{35}$$

$$\mathbf{C} = \mathbf{K} - \rho h \hat{\mathbf{K}}, \quad \mathbf{D} = \mathbf{B} - \rho h \hat{\mathbf{B}}, \tag{36}$$

equation (30) can be written as

$$\mathbf{A}\ddot{\mathbf{V}} + \mathbf{C}\mathbf{V} + \mathbf{D}\dot{\mathbf{V}} = \mathbf{0}, \tag{37}$$

or after transformation into state (4×4) space as

$$\begin{bmatrix} \mathbf{I} & \mathbf{0} \\ \mathbf{0} & \mathbf{A} \end{bmatrix} \begin{bmatrix} \dot{\mathbf{V}} \\ \ddot{\mathbf{V}} \end{bmatrix} = \begin{bmatrix} \mathbf{0} & \mathbf{I} \\ -\mathbf{C} & -\mathbf{D} \end{bmatrix} \begin{bmatrix} \mathbf{V} \\ \dot{\mathbf{V}} \end{bmatrix}, \tag{38}$$

where $\mathbf{I}$ is the unit matrix (2×2).

Left multiplication by the inverse matrix $\mathbf{A}^{-1}$ yields

$$\begin{bmatrix} \dot{\mathbf{V}} \\ \ddot{\mathbf{V}} \end{bmatrix} = \begin{bmatrix} \mathbf{0} & \mathbf{I} \\ -\mathbf{A}^{-1}\mathbf{C} & -\mathbf{A}^{-1}\mathbf{D} \end{bmatrix} \begin{bmatrix} \mathbf{V} \\ \dot{\mathbf{V}} \end{bmatrix}, \tag{39}$$

which is also possible to rewrite as

$$\dot{\mathbf{y}} = \hat{\mathbf{A}}\mathbf{y}, \tag{40}$$

where the following notation was introduced

$$\hat{\mathbf{A}} = \begin{bmatrix} \mathbf{0} & \mathbf{I} \\ -\mathbf{A}^{-1}\mathbf{C} & -\mathbf{A}^{-1}\mathbf{D} \end{bmatrix}, \quad \mathbf{y} = \begin{bmatrix} \mathbf{V} \\ \dot{\mathbf{V}} \end{bmatrix}. \tag{41}$$

Assuming

$$\mathbf{y} = \mathbf{y}_0 \mathrm{e}^{st}, \quad \mathbf{V} = \mathbf{V}_0 \mathrm{e}^{st} \tag{42}$$

for the dynamic response of the structure, the solution is finally given by the numerical calculation of the eigenvalues s and eigenvectors $\mathbf{y}_0$ for the eigenvalue problem

$$(\hat{\mathbf{A}} - s\mathbf{I})\mathbf{y}_0 = \mathbf{0}. \tag{43}$$

Calculation of the eigenvalues s and eigenmodes $\mathbf{V}_0^T = (V_{01}, V_{02})$ enables us to study the dependence of the frequency-modal and damping characteristics of the system on various physical and physiological parameters (e.g., on the geometry of the glottis, on the shape of the vocal folds, on the glottal flux, etc.). In this way, it is also possible to calculate a critical flow velocity U_0 at which the system becomes unstable, thus simulating the threshold of phonation. This situation happens when the real part of the eigenvalue changes sign from negative ($\Re\mathrm{e}(s) < 0$) to positive ($\Re\mathrm{e}(s) > 0$). The eigenvalues s and eigenmodes $\mathbf{V}_0$ will be further expressed as the complex eigenfrequencies $f = \Re\mathrm{e}(f) + \mathrm{i}\Im\mathrm{m}(f)$, defined by $f = s/2\pi$, and the dimensionless complex eigenmodes $\hat{\mathbf{V}}_0^T = (V_{01}, V_{02}/L)$.

5. NUMERICAL ANALYSIS

5.1. Input Data for Numerical Calculations

Generally, in biomechanics it is not easy to measure, and even to find in the literature, reliable material properties of biological tissues. In the case of the vocal folds the situation is further complicated due to the lack of knowledge of the living tissue geometry, which depends on the tension in the vocal fold and varies with the phonation frequency (pitch), loudness as well as mode of phonation (Hirano 1974, 1975). In order to link our model to the properties of the real vocal folds, the dimensions and the geometry were, as a first approximation, taken from a coronal view of the vocal folds published by Berry *et al.* (1994, p. 3598, Figure 3). This shape of the vocal fold was approximated by a parabolic function

$$a(x) = -159{\cdot}861(x - 5{\cdot}812 \times 10^{-3})^2 + 5{\cdot}4 \times 10^{-3}(\mathrm{m}). \tag{44}$$

The density, length of the glottal region and length of the vocal folds were taken as follows: $\rho_h = 1020\,\mathrm{kg/m^3}$, as measured by Perlman & Durham (1987), $L = 6{\cdot}8\,\mathrm{mm}$ and $h = 18\,\mathrm{mm}$, which approximately correspond to male vocal folds (Dedouch *et al.* 1999). Using these data and equation (44), the eccentricity $e = 7{\cdot}7106 \times 10^{-4}\,\mathrm{m}$, the total mass $m = 4{\cdot}8116 \times 10^{-4}\,\mathrm{kg}$ and the moment of inertia $I = 2{\cdot}3508 \times 10^{-9}\,\mathrm{kg\,m^2}$ were calculated, and thus according to equations (1) and (6) the mass matrix $\mathbf{M}$ was determined.

The vocal-fold shape, the dimensions and the calculated position of the centre of gravity T are shown in Figure 4.

The height H_0 of the channel according to Figure 2 is given by

$$H_0 = \max a(x) + g, \tag{45}$$

where $x \in \langle 0, L \rangle$ and g is the glottal half-width, which is one of the most important control parameters of the system. The glottal half-width g is associated with the degree of the so-called adduction of the vocal folds. The air density was taken in the calculated examples as $\rho = 1{\cdot}2\,\mathrm{kg/m^3}$.

A tuning procedure was used to adjust the stiffness k of the elastic foundation and the damping coefficients ε_1, ε_2 in equations (6) and (7). The tuning procedure was performed in order to approximate the fundamental natural frequency, $\mathfrak{Im}(f_1)$, and 3 dB half-power bandwidths Δf_1 and Δf_2 of both resonances of the model by values measured on true vocal folds (Kaneko *et al.* 1987; Švec *et al.* 2000). Mathematical background of the tuning procedure is described in more detail in Appendix C.

Because there is large dispersion in the empirical data, especially in the damping properties of the vocal folds, the tuning procedure was applied on the mechanical system *in vacuo* (for $\rho = 0$) excluding in this way the influence of the glottal half-width g on the coefficients ε_1, ε_2. First, by changing the stiffness k of the foundation, the desired fundamental natural frequency $\mathfrak{Im}(f_1)$ was tuned and adjusted in the model. Then, the coefficients ε_1, ε_2 of the linear damping approximation (7) were calculated according to the following approximate formulas derived in Appendix C:

$$\varepsilon_1 = 2\pi \frac{\Delta f_1 \mathfrak{Im}^2 f_2 - \Delta f_2 \mathfrak{Im}^2 f_1}{\mathfrak{Im}^2 f_2 - \mathfrak{Im}^2 f_1} \quad \text{and} \quad \varepsilon_2 = \left(\frac{1}{2\pi}\right) \frac{\Delta f_1 - \Delta f_2}{\mathfrak{Im}^2 f_1 - \mathfrak{Im}^2 f_2}. \tag{46}$$

The tuning procedure was applied on three sets of measured data [see Table 1 in Švec *et al.* (2000) and Figures 25·9–25·10 in Kaneko *et al.* (1987)], and three mathematical models of the vocal folds denoted by S1, K1 and K2 were created. The calculated parameters k, ε_1 and ε_2 of these models and their fundamental dynamical properties are summarized in Tables 1–3 including the damping ratios

$$D_i = \Delta f_i / (2\sqrt{[\mathfrak{Re}^2(f_i)] + [\mathfrak{Im}^2(f_i)]}$$

For all the second-mode natural frequencies, $\mathfrak{Im}(f_2)$, in Tables 1–3, we have approximately $\mathfrak{Im}(f_2) : \mathfrak{Im}(f_1) \approx 3 : 2$, which is in good agreement with experimental results (Švec *et al.* 2000).

The eigenmodes for the vocal-fold-shaped element vibrating *in vacuo* are shown in Figure 5. Because they do not depend on the stiffness of the elastic foundation (see

TABLE 1

Frequency and damping characteristics of the model S1 ($k = 420\,\mathrm{N/m}$, $\varepsilon_1 = 113{\cdot}44\,\mathrm{rad/s}$, $\varepsilon_2 = 146{\cdot}30 \times 10^{-6}\,\mathrm{s/rad}$)

Measured data (Švec *et al.* 2000)		
$\mathfrak{Im}(f_1) = 114\,\mathrm{Hz}$	$\Delta f_1 = —$	$D_1 = —$
$\mathfrak{Im}(f_2) = 171\,\mathrm{Hz}$	$\Delta f_2 = 44\,\mathrm{Hz}$	$D_2 = 0{\cdot}13$
Modelled data for $\rho = 0$		
$\mathfrak{Im}(f_1) = 114.5\,\mathrm{Hz}$	$\Delta f_1 = 30{\cdot}3\,\mathrm{Hz}$	$D_1 = 0{\cdot}130$
$\mathfrak{Im}(f_2) = 168.5\,\mathrm{Hz}$	$\Delta f_2 = 44{\cdot}6\,\mathrm{Hz}$	$D_2 = 0{\cdot}132$

TABLE 2

Frequency and damping characteristics of the model K1 ($k = 314{\cdot}78$ N/m, $\varepsilon_1 = 123$ rad/s, $\varepsilon_2 = 55{\cdot}5 \times 10^{-6}$ s/rad)

Measured data (Kaneko *et al.* 1987)		
$\Im\mathfrak{m}(f_1) = 100$ Hz	$\Delta f_1 \approx 23$ Hz	$D_1 = 0{\cdot}12$
$\Im\mathfrak{m}(f_2) \approx 160-190$ Hz	$\Delta f_2 \approx 29$ Hz	$D_2 \approx 0{\cdot}08$
Modelled data for $\rho = 0$		
$\Im\mathfrak{m}(f_1) = 99{\cdot}3$ Hz	$\Delta f_1 = 23{\cdot}1$ Hz	$D_1 = 0{\cdot}116$
$\Im\mathfrak{m}(f_2) = 146{\cdot}5$ Hz	$\Delta f_2 = 27{\cdot}1$ Hz	$D_2 = 0{\cdot}092$

TABLE 3

Frequency and damping characteristics of the model K2 ($k = 964{\cdot}02$ N/m, $\varepsilon_1 = 175$ rad/s, $\varepsilon_2 = 6{\cdot}21 \times 10^{-6}$ s/rad)

Measured data (Kaneko *et al.* 1987)		
$\Im\mathfrak{m}(f_1) = 175$ Hz	$\Delta f_1 = 29$ Hz	$D_1 = 0{\cdot}08$
$\Im\mathfrak{m}(f_1) \approx 240-270$ Hz	$\Delta f_2 \approx 30$ Hz	$D_2 \approx 0{\cdot}06$
Modelled data for $\rho = 0$		
$\Im\mathfrak{m}(f_1) = 174{\cdot}4$ Hz	$\Delta f_1 = 29{\cdot}04$ Hz	$D_1 = 0{\cdot}083$
$\Im\mathfrak{m}(f_2) = 257{\cdot}1$ Hz	$\Delta f_2 = 30{\cdot}4$ Hz	$D_2 = 0{\cdot}059$

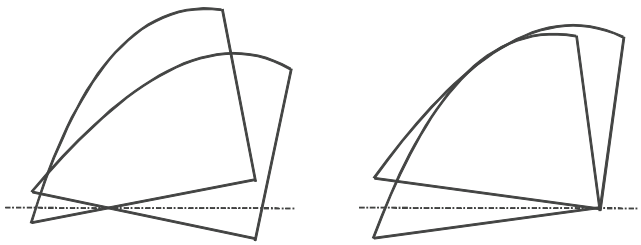

(a) (b)

Figure 5. Eigenmodes for the models vibrating *in vacuo* ($\rho = 0$): (a) $\hat{\mathbf{V}}_{0,1}$; (b) $\hat{\mathbf{V}}_{0,2}$; (exaggerated amplitudes).

Appendix C), they are identical for all the models investigated: S1, K1 and K2. Both eigenmodes are combinations of rotational and translational motion.

5.2. Results of Numerical Calculations

5.2.1. Mathematical model S1

Typical results of computed complex eigenfrequencies, $f = \Re\mathfrak{e}(f) + \mathrm{i}\Im\mathfrak{m}(f)$, as functions of the mean flow velocity U_0 are shown in Figures 6 and 8 for two different values of the glottal half-width g.

For a small gap $g = 0{\cdot}16$ mm (see Figure 6) the imaginary part of the first frequency, $\Im\mathfrak{m}(f_1)$, rapidly decreases when the flow velocity U_0 increases. This frequency reaches the

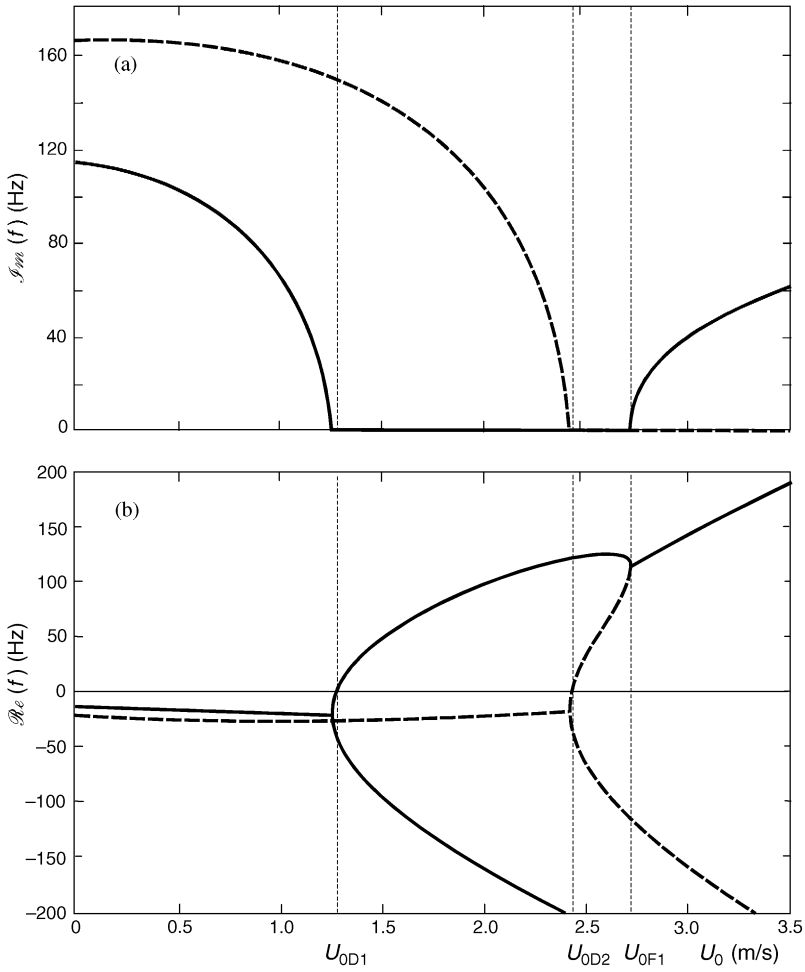

Figure 6. Complex eigenfrequencies $f_j = \mathfrak{Re}(f_j) + \mathrm{i}\mathfrak{Im}(f_j)$ $(j = 1, 2)$ for the model S1 as functions of the flow velocity U_0 for the gap $g = 0{\cdot}16$ mm: ———, $j = 1$ (1st mode); — — —, $j = 2$ (2nd mode).

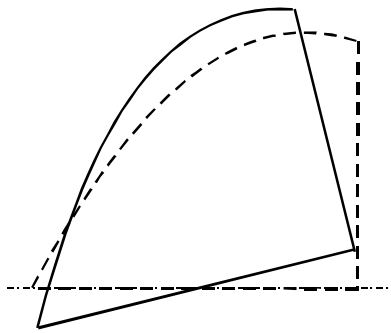

Figure 7. Eigenmode $\hat{\mathbf{V}}_{0,1}$ at the critical flow velocity for divergence for the model S1 and the gap $g = 0{\cdot}16$ mm.

zero value $[\mathfrak{Im}(f_1) = 0$ and $\mathfrak{Re}(f_1) = 0]$ at the critical flow velocity for divergence $U_{0D1} \approx 1{\cdot}267$ m/s when the divergence instability appears in the system. For higher flow velocities $(U_0 > U_{0D1})$ $\mathfrak{Im}(f_1) = 0$ and $\mathfrak{Re}(f_1) > 0$, the divergence instability for the

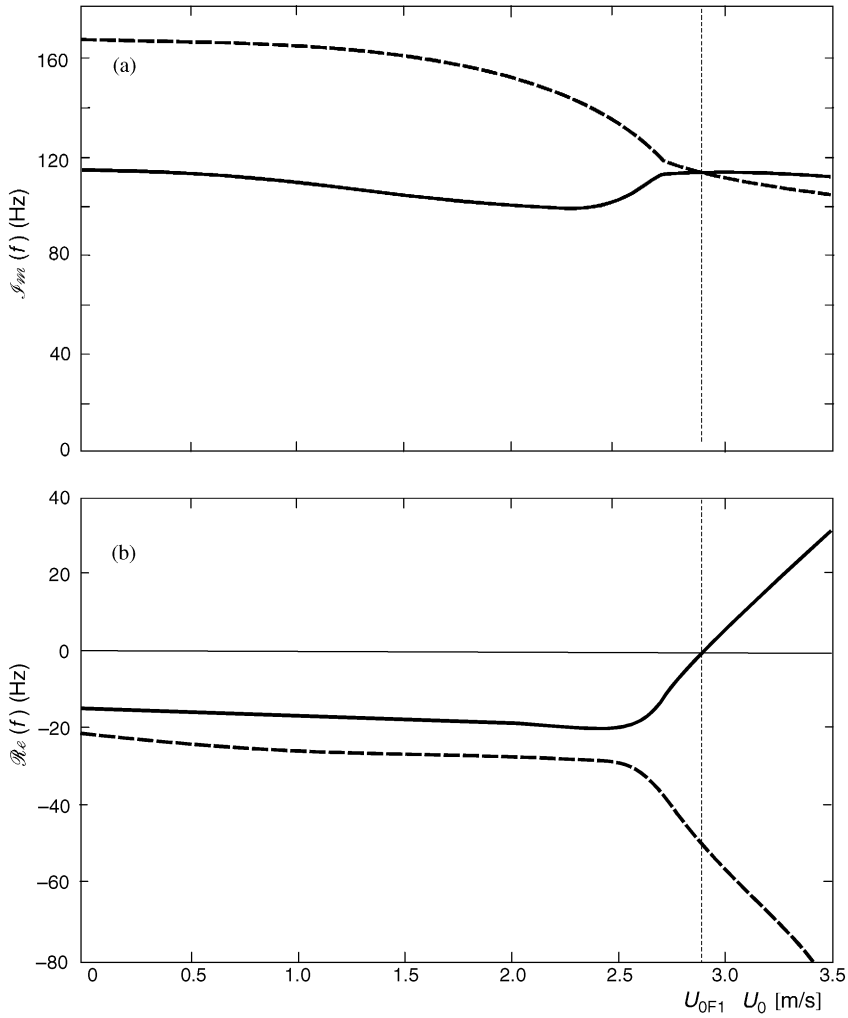

Figure 8. Complex eigenfrequncies $f_j = \mathfrak{Re}(f_j) + \mathrm{i}\mathfrak{Im}(f_j)$ $(j = 1, 2)$ for the model S1 as functions of the flow velocity U_0 for the gap $g = 0{\cdot}3$ mm: ———, $j = 1$ (1st mode); — — —, $j = 2$ (2nd mode).

first-mode shape of vibration takes place, which means that, according to equation (42), the displacements of the vibrating element are increasing monotonically in time and the system is statically unstable (no oscillation arises here). Critical flow velocity for divergence of the second mode is near the value $U_{0D2} \approx 2{\cdot}42$ m/s. For higher flow velocities, $U_0 > U_{0F1} \approx 2{\cdot}72$ m/s, a coupled-mode flutter theoretically occurs, when $\mathfrak{Im}(f_1) > 0$ and $\mathfrak{Re}(f_1) > 0$. The flutter instability means that according to equation (42) the amplitudes of the vibrating element increase exponentially in time, the system is dynamically unstable and oscillation takes place. The corresponding oscillation frequency $f_{\text{flutter}} = \mathfrak{Im}(f_1)$ is called the flutter frequency. It can be said that the flutter frequency defined here from the aeroelastic point of view corresponds to the phonation or pitch frequency used in speech terminology. [Apparently, the term "flutter" has a different meaning in voice/speech literature, (see, e.g., Titze 1994), than in the aeroelastic literature. For more details about various static and oscillatory types of instabilities from the aeroelastic point of view, see, e.g., Païdoussis (1998)].

TABLE 4

Normalized eigenmodes $\hat{\mathbf{V}}_0$ for zero-flow velocity and for critical flow velocity for divergence for the model S1 and the gap $g = 0{\cdot}16\,\text{mm}$

Mode	$U_0 = 0$	$U_0 = 1{\cdot}267\,\text{m/s} \approx U_{0D}$
$\hat{\mathbf{V}}_{0,1}$	$\begin{pmatrix} 1 \\ 0{\cdot}174 + \text{i}\ 3.1 \times 10^{-4} \end{pmatrix}$	$\begin{pmatrix} 1 \\ -0{\cdot}040 \end{pmatrix}$
$\hat{\mathbf{V}}_{0,2}$	$\begin{pmatrix} 1 \\ -0{\cdot}478 + \text{i}\ 5{\cdot}8 \times 10^{-4} \end{pmatrix}$	$\begin{pmatrix} 1 \\ -0{\cdot}378 + \text{i}\ 0{\cdot}026 \end{pmatrix}$

TABLE 5

Normalised eigenmodes $\hat{\mathbf{V}}_0$ for zero-flow velocity and for critical flow velocity for flutter for the model S1 and the gap $g = 0{\cdot}3\,\text{mm}$

Mode	$U_0 = 0$	$U_0 = 2{\cdot}91\,\text{m/s} \approx U_{0F}$
$\hat{\mathbf{V}}_{0,1}$	$\begin{pmatrix} 1 \\ 0{\cdot}174 + \text{i}\ 1{\cdot}7 \times 10^{-4} \end{pmatrix}$	$\begin{pmatrix} 1 \\ -0{\cdot}298 - \text{i}\ 0{\cdot}067 \end{pmatrix}$
$\hat{\mathbf{V}}_{0,2}$	$\begin{pmatrix} 1 \\ -0{\cdot}480 + \text{i}\ 3{\cdot}2 \times 10^{-4} \end{pmatrix}$	$\begin{pmatrix} 1 \\ -0{\cdot}275 + \text{i}\ 0{\cdot}077 \end{pmatrix}$

The corresponding normalized, generally complex, eigenmodes $\hat{\mathbf{V}}_0$ for the model S1 and the glottal half-width $g = 0{\cdot}16\,\text{mm}$ are presented in Table 4 for $U_0 = 0$ and U_{0D1}. At the critical flow velocity for divergence $U_0 = U_{0D1}$ the rotation prevails for the first-mode shape of vibration. This unstable eigenmode at the critical flow velocity for divergence ($U_{0D1} \approx 1{\cdot}267\,\text{m/s}$) is shown in Figure 7. The vocal fold is, in accordance with equation (42), sucked into the glottal gap, because for $U_0 > U_{0D1}$ $\Im\mathfrak{m}(f_1) = 0$ and $\Re\mathfrak{e}(f_1) > 0$.

For wider glottal half-width $g = 0{\cdot}3\,\text{mm}$ (see Figure 8) the static divergence instability does not occur, and the critical flow velocity becomes the velocity $U_0 = U_{0F1} \approx 2{\cdot}91\,\text{m/s}$ for classical single-mode flutter. For the velocity U_{0F1} both natural frequencies are identical [$\Im\mathfrak{m}(f_1) = \Im\mathfrak{m}(f_2) > 0$] and $\Re\mathfrak{e}(f_1) = 0$. For higher air-flow velocities, $U_0 > U_{0F1}$, the amplitudes of vibration increase with time because $\Re\mathfrak{e}(f_1) > 0$ and the system is dynamically unstable. This regime offers the best conditions for self-sustained oscillations of the vocal folds, because the energy of the flowing air is transferred into the vibrations of the vocal folds.

The corresponding normalized eigenmodes $\hat{\mathbf{V}}_0$ are presented in Table 5 for $U_0 = 0$ and U_{0F1}. For zero-flow velocity, when only the fluid added mass influences the mechanical part of the model by the matrix $\hat{\mathbf{M}}$ in equation (30), the eigenmodes are not substantially influenced by the gap size g (compare Tables 4 and 5). With regard to the critical flow

velocity for flutter $U_0 = U_{0F1}$, both eigenmodes in Table 5 are very close, and they are combinations of translational and rotational motion. The motion of the vocal-fold-shaped element at the critical flow velocity for flutter ($U_{0F1} = 2{\cdot}91$ m/s) is shown in Figure 9, where the displacement $\Re\mathrm{e}(\hat{\mathbf{V}}_0 \mathrm{e}^{st})$ during one vibration cycle is presented. Due to the fluid-structure interaction, there is no exact position of the nodal point, which results in a wave-like motion of the vocal folds.

The results of calculations of the instability boundaries (U_{0D1} and U_{0F1}) for the system S1 are shown as functions of the glottal half-width g in Figure 10 in a stability map for the system with and without dissipation. For the system with proportional damping ($\varepsilon_1 > 0, \varepsilon_2 > 0$) and for narrow glottal gaps ($g \lesssim 0{\cdot}2$ mm), the lowest stability boundary is given by the critical flow velocity U_{0D1} for divergence. For wider gaps ($g > 0{\cdot}2$ mm), the lowest stability boundary is given by the critical flow velocity U_{0F1} for flutter. For the undamped system ($\varepsilon_1 = \varepsilon_2 = 0$), the stability boundaries for divergence (U_{0D1}) are unchanged, because the divergence is in principle a static phenomenon and is not influenced by damping. The stability boundaries for the occurrence of flutter (U_{0F1}) are lower in this case, however. That reflects the known fact that the lower damping of the vocal folds is more advantageous for phonation, because a lower air-flow velocity is needed for starting the instability. Assuming, for instance, the maximum volume flow rate: $Q_{\max} = 1$ l/s as an approximate physiological boundary, it can be implied that, for example, for the glottal gap (abduction) $2g = 2$ mm the flow source comparable with the human lungs would not be able to start and support the phonation. The reason is that the critical air-flow velocity for flutter $U_{0F1} \approx 8{\cdot}9$ m/s presented in Figure 10 for $g = 1$ mm is

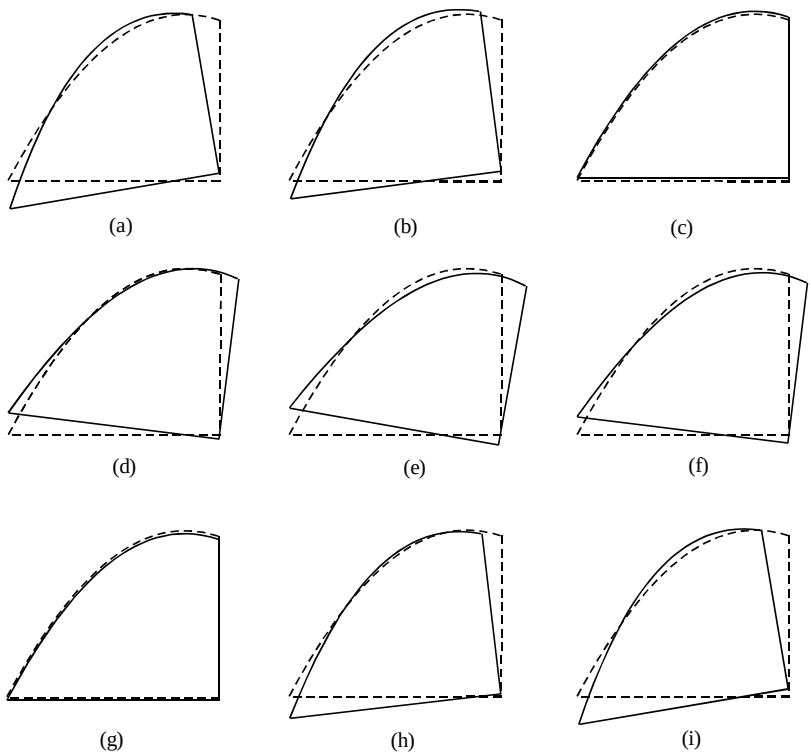

Figure 9. Motion of the vocal-fold-shaped element during one period of vibration at the critical flow velocity for flutter for the model S1 and the gap $g = 0{\cdot}3$ mm.

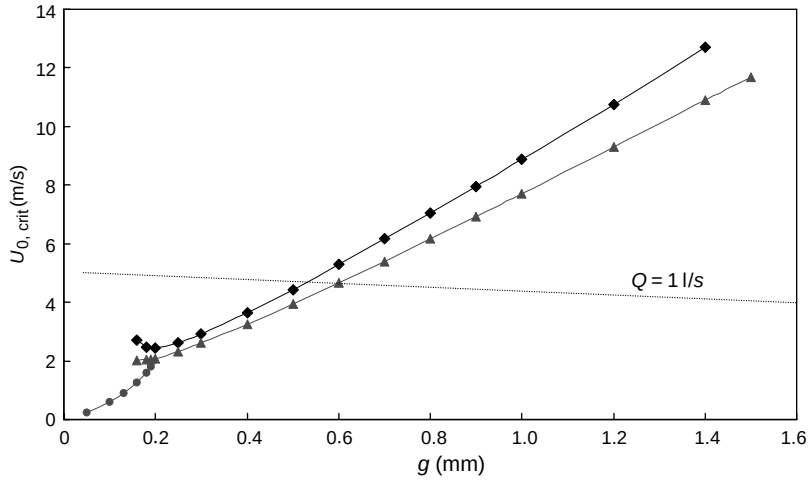

Figure 10. Stability map for the model S1: ●, critical flow velocity U_{0D1} for divergence; ▲, critical flow velocity U_{0F1} for flutter for the system without damping ($\varepsilon_1 = 0, \varepsilon_2 = 0$); ◆, critical flow velocity U_{0F1} for flutter for the system with proportional damping ($\varepsilon_1 = 113{\cdot}44\,\text{rad/s}$, $\varepsilon_2 = 146{\cdot}30 \times 10^{-6}\,\text{s/rad}$).

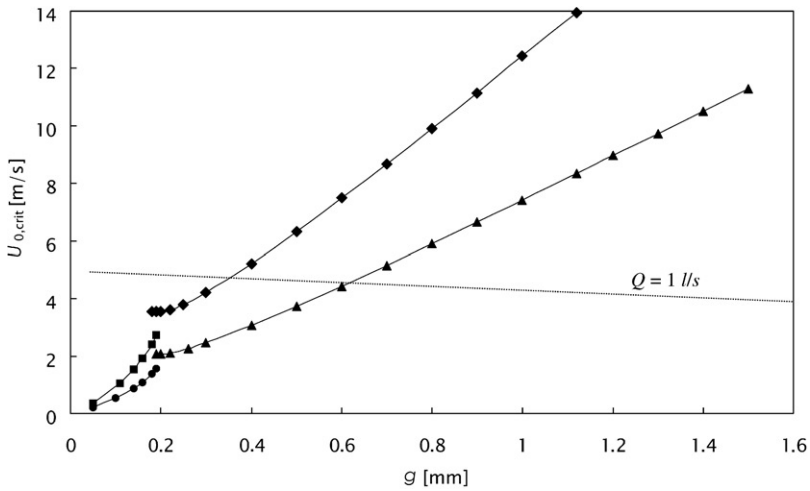

Figure 11. Stability map for the models K1 and K2: ●, critical flow velocity U_{0D1} for divergence of model K1; ■, critical flow velocity U_{0D1} for divergence of K2; ▲, critical flow velocity U_{0F1} for flutter of model K1; ◆, critical flow velocity U_{0F1} for flutter of model K2.

more than two times higher than the flow velocity $U_{0\max} \approx 4{\cdot}33\,\text{m/s}$ given according to equations (29) and (45) as

$$U_{0\max} = Q_{\max}/[2(\max a(x) + g)h], \quad x \in \langle 0, L \rangle. \tag{46'}$$

The flow velocity U_{0max} for the physiological boundary considered is shown as function of g in Figures 10 and 11 as well. The larger is the glottal half-width g the higher is the critical flow velocity for reaching the instability, and thus the more difficult is to initialize the phonation.

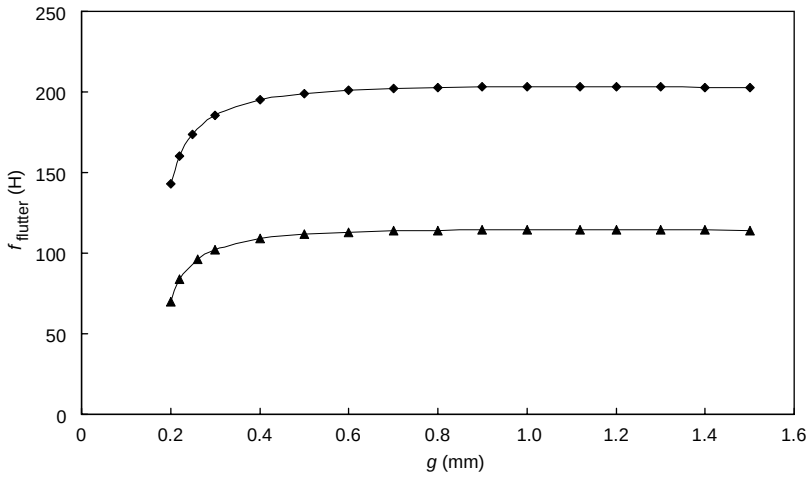

Figure 12. Flutter frequencies at $U_0 = U_{0F1}$ for the models K1 and K2 as functions of the gap g: ▲, model K1; ◆, model K2.

5.2.2. *Mathematical models* K1 *and* K2

The results of calculations for the Kaneko data K1 and K2 are presented in Figures 11 and 12. The stability map of the system is shown in Figure 11 in a similar way as used in the previous model S1. The stability boundaries for the Kaneko data K1 and K2 are generally in qualitative agreement with the results for the model S1. Moreover, from Figure 11 it is clear that the higher is the fundamental natural frequency [$\Im\mathrm{m}(f_1) = 100$ Hz for K1 and $\Im\mathrm{m}(f_1) = 175$ Hz for K2], the higher are the critical flow velocities for divergence as well as for flutter, and thus the more difficult it is to start the phonation.

The flutter frequencies, i.e., $f_{\mathrm{flutter}} = \Im\mathrm{m}(f_1)$, for the critical flow velocity $U_0 = U_{0F1}$, are presented in Figure 12 as functions of the glottal half-width g. It can be seen that the wider the glottal gap, the higher is the flutter frequency. Approximately, for $g > 0{\cdot}4$ mm, however, the flutter frequency approaches a nearly constant value, which is somewhat higher than the first zero-flow natural frequency of the system. Thus, according to the aeroelastic model developed, the flutter frequency is generally different from the fundamental natural frequency of the vocal-fold-shaped vibrating element.

Additional analysis of aeroelastic behaviour of the vocal-fold-shaped vibrating element was performed by the authors (Horáček & Švec 2001) recently, calculating more examples for three different shapes of the vocal folds. In addition to the shape with an intermediate bulging given by equation (44), another two geometries were considered, which approximately correspond to female and male vocal-fold shapes, in accordance with Titze (1989):

$$a_f(x) = 0.77120x \text{ (m)} \quad \text{and} \quad a_m(x) = -216{\cdot}263x^2 + 2{\cdot}2418 \text{ (m)}. \tag{47}$$

It was revealed that, according to the theoretical model developed, the flutter instability boundaries are lower for the female (linear) geometry $a_f(x)$ of the vocal folds, which appears to sustain the phonation more easily.

6. GENERAL DISCUSSION

The model presented here is designed to study the frequency-modal and damping characteristics of the vocal-fold vibration as well as their phonatory threshold states.

These characteristics are very important for understanding the mechanism and conditions for the vocal-fold oscillations under conditions where detailed empirical data is lacking. The preliminary analysis presented using this model, reveals a behaviour which is in reasonable qualitative agreement with the clinical observations as well as with the dynamical properties of the Ishizaka–Flanagan two-mass model of the vocal folds as analysed by Ishizaka (1988). Ishizaka obtained similar variation of both natural frequencies with increasing air-flow velocity in the glottis, as shown here in Figure 8, including the flutter-type instability. The divergence-type instabilities were not described by Ishizaka, however. Our results reveal that a divergence type of instability takes place in the case of relatively small glottal gaps (g) at low flow velocities, and according to the linear approach presented it results in a slight deformation of the vocal folds without any vibration. When the flow velocity is increased above another threshold value, the divergence instability is replaced by the flutter type of instability and the vocal folds start to oscillate.

For showing an approximate quantitative agreement of the preliminary results with other studies, the stability map in Figure 11 computed for the K1 model with the fundamental natural frequency 100 Hz will be used. For example, the calculated critical flow velocity for flutter $U_{0F1} \cong 3\,\mathrm{m/s}$ for the glottal half-width $g = 0{\cdot}4\,\mathrm{mm}$ gives, according to equations (29), (44) and (45), the corresponding glottal volume velocity $Q_F \cong 0{\cdot}63\,\mathrm{l/s}$. This is only slightly higher than the value encountered in the literature for male adults (Pelorson *et al.* 1995). Using Bernoulli's law and the continuity equation, the pressure difference between the inlet ($x = 0$) and outlet ($x = L$) of the glottal region can be expressed as

$$\Delta P = 1/2\rho U_0^2\{H_0/[H_0 - a(L)]\}^2, \tag{48}$$

where $H_0(g)$ and $a(L)$ are defined by equations (44) and (45), respectively. Substituting $g = 0{\cdot}4\,\mathrm{mm}$, $U_0 = U_{0F1} \cong 3\,\mathrm{m/s}$, $\rho = 1{\cdot}2\,\mathrm{kg/m^3}$ and $L = 6{\cdot}8\,\mathrm{mm}$, the so-called phonation threshold pressure $\Delta P_{th} = 588\,\mathrm{Pa}$ can be estimated from here. This value is higher than the value encountered in the literature for humans [around $3\,\mathrm{cmH_2O}$, thus approximately 300 Pa, for the phonatory frequencies around 100 Hz in accordance with Verdolini-Marston *et al.* (1990)], however, not much higher than, for example, the phonation pressure $\Delta P_{th} = 450-500\,\mathrm{Pa}$ calculated for $g = 0{\cdot}4-0{\cdot}6\,\mathrm{mm}$ by Lucero (1998) for much smaller vocal-fold-shaped element ($L = 6\,\mathrm{mm}$, $h = 14\,\mathrm{mm}$ and $a(L) \cong 1{\cdot}2\,\mathrm{mm}$) using a completely different model for vocal-fold vibration. Finally, we can note, that in the case of the flutter instability considered, Bernoulli's law and the continuity equation give the maximum flow velocity in the narrowest part of glottis 43.5 m/s. This value is in the range of air-flow velocities, which justifies the assumption of fluid incompressibility.

The model is designed as a first approximation of the vocal-fold vibratory system. Certain simplifications are incorporated in the model; e.g., the elastic properties for the pitch and heave motion are not separately modifiable (like in the Liljencrants and Ishizaka–Flanagan types of models) but are rather determined by the mass distribution of the vibrating element and the properties of the elastic foundation. Furthermore, the viscous fluid forces are not taken into account, and only small disturbances of the air-flow velocity are allowed [corresponding to the condition $\tilde{u}(\partial\tilde{u}/\partial x) \to 0$ used in equation (13)]. The latter condition means that the model is restricted to simulating phonation threshold states, excluding the adjustments with closed glottis and the collision of the two vocal folds. The model is able to provide information, e.g. on conditions for a soft voice onset or for breathy voicing when the glottis never closes completely. This might be done by calculating the critical parameters at which the system loses stability.

Simultaneously with the statement that further improvements of the present model are possible, it is important to realize that the limitations of the theory presented here arise mainly in the fluid part of the problem. The mechanical part of the vocal-fold model could be modified much more easily; e.g., (i) to replace the continuous elastic foundation by two or more discrete springs, enabling an independent tuning of both natural frequencies, (ii) to introduce more degrees of freedom in the mechanical system, (iii) to include stiffness and damping nonlinearities in a similar way as in our previous paper (Horáček *et al*. 1996), or even (iv) to include a model of soft impacts (Peterka & Szöllös 1999) in the numerical simulation of the vocal-folds oscillation.

7. CONCLUSIONS

A newly developed theoretical aeroelastic model of vocal-folds vibration was presented, which was adjusted to approximately correspond to the measured properties of the vocal folds. The design of the model enables the study of the influence of various geometrical, material and fluid flow parameters on the dynamical characteristics and aeroelastic stability of the system. The mass, stiffness and damping matrices of the mechanical part of the model are simply related to the physiological data.

Preliminary numerical calculations of the vibration characteristics and stability boundaries proved that the present aeroelastic model of vocal-fold vibration (i) shows dynamical behaviour which approximately corresponds the dynamical behaviour of the real vocal folds, (ii) shows stability boundaries which approximately correspond to the measured thresholds of phonation in humans, (iii) reasonably relates the conditions and mechanism for starting the vocal-fold vibration to the states at which the stability boundaries of the aeroelastic system are crossed and the energy transfer from the air-flow to the vocal folds starts self-sustained oscillations.

ACKNOWLEDGEMENTS

The authors acknowledge the financial support of the Grant Agency of the Czech Republic by project No 106/98/K019, on Mathematical and physical modelling of vibroacoustic systems in biomechanics of voice and hearing.

REFERENCES

ALIPOUR, F. & SCHERER, R. C. 2000 Vocal fold bulging effects on phonation using a biophysical computer model. *Journal of Voice* **14,** 470–483.

BERRY, D. A., HERZEL, H., TITZE, R. & KRISCHER, K. 1994 Interpretation of biomechanical simulations of normal and chaotic vocal fold oscillations with empirical eigenfunctions. *Journal of the Acoustical Society of America* **95,** 3595–3604.

BERRY, D. A. & TITZE, R. 1996 Normal modes in continuum model of vocal fold tissues. *Journal of the Acoustical Society of America* **100,** 3345–3354.

DEDOUCH, K., VAMPOLA, T. & ŠVEC, J. 1999 Influence of the length changes on modal properties of the vocal fold tissues. In *Proceedings of the of 15th Conference Computational Mechanics'99*, October 18–20, 1999, Nečtiny (ed. J. Křen), pp. 39–46. University of West Bohemia, Pilsen, Czech Republic.

DE VRIES, M. P., SCHUTTE, H. K. & VERKERKE, G. J. 1999 Determination of parameters for lumped parameter models of the vocal folds using a finite-element method approach. *Journal of the Acoustical Society of America* **106,** 3620–3628.

FLANAGAN, J. L. & LANDGRAF, L. L. 1968 Self oscillating source for vocal tract synthesizers. *IEEE Transactions on Audio and Electroacoustics* **AU-16,** 57–64.

HIRANO, M. 1974 Morphological structure of the vocal cord as a vibrator and its variations. *Folia Phoniatrica* **26,** 89–94.

HIRANO, M. 1975 Phonosurgery: basic and clinical investigations. *Otologia (Fukuoka)* **21**(Suppl.1), 239–442.

HORÁČEK, J., SIMERSKÁ, C. & BENEŠ, V. 1996 Effects of structural nonlinearities in an aeroelastic dynamic system. In *Proceedings of the 2nd European Nonlinear Oscillation Conference*, September 9–13, 1996, Prague (eds L. Půst & F. Peterka), Vol. 1, pp. 195–198. Institute of Thermomechanics, Academy of Sciences of the Czech Republic.

HORÁČEK, J. & ŠVEC, J. G. 2000 Aeroelastic model of vocal-fold vibration. In *Flow-Induced Vibration* (eds S. Ziada & T. Staubli), pp. 419–425. Rotterdam: A.A. Balkema.

HORÁČEK, J. & ŠVEC, J. G. 2001 Analysis of aeroelastic behaviour of the vocal-fold-shaped vibrating element. In *Vth International Conference Advances in Quantitative Laryngoscopy, Voice and Speech Research*, 27–28 April 2001, Groningen (CD-ROM compiled by H. Schutte). Groningen Voice Research Lab, University of Groningen, The Netherlands.

HORÁČEK, J., VESELÝ, J. & URUBA, V. 1997 Aeroelastic instability of a flexibly supported plate vibrating in a channel. *Engineering Mechanics* **4,** 335–348 (in Czech).

INMAN, D. J. 1989 *Vibration: with Control, Measurement, and Stability*. Englewood Cliffs, NJ: Prentice-Hall.

ISHIZAKA, K. & FLANAGAN, J. L. 1972 Synthesis of voiced sounds from a two-mass model of the vocal cords. *The Bell System Technical Journal* **51,** 1233–1268.

ISHIZAKA, K. 1988 Significance of Kaneko's measurement of natural frequencies of the vocal folds. In *Vocal Folds Physiology*, Vol. 2: Voice production mechanisms and functions (ed. O. Fujimura), pp. 181–190. New York: Raven Press.

KANEKO, T., MASUDA, T., SHIMADA, A., SUZUKI, H., HAYASAKI, K. & KOMATSU, K. 1987 Resonance characteristics of human vocal fold in vivo and in vitro by an impulse excitation. In *Laryngeal Function in Phonation and Respiration* (eds T. Baer, C. Sasaki & K.S. Haris). pp. 349–365. Boston: A College-Hill Press/Little, Brown and Company.

LILJENCRANTS, J. 1991 A translating and rotating mass model of the vocal folds. In *Speech Transmission Laboratory—Quarterly Progress and Status Report* 1/1991, Stockholm, pp. 1–18.

LOUS, N. J. C., HOFMANS, G. C. J., VELDHUIS, R. N. J. & HIRSCHBERG, A. 1998 A symmetrical two-mass vocal-fold model coupled to vocal tract and trachea, with application to prosthesis design. *Acta Acustica* **84,** 1135–1150.

LUCERO, J. C. 1998 Optimal glottal configuration for ease of phonation. *Journal of Voice* **12,** 151–158.

LUCERO, J. C. 1999 A theoretical study of the hysteresis phenomenon at vocal fold oscillation onset–offset. *Journal of the Acoustical Society of America* **105,** 423–431.

MERGELL, P. 1998 Nonlinear Dynamics of Phonation: High-Speed Glottography and Biomechanical Modelling of Vocal Fold Oscillations (Dissertation). Aachen: Shaker Verlag.

NORTON, M. P. 1989 Fundamentals of Noise and Vibration Analysis for Engineers. Cambridge: Cambridge University Press.

PAÏDOUSSIS, M. P. 1998 *Fluid–Structure Interactions. Slender Structures and Axial Flow*, Vol. 1. London: Academic Press.

PERLMAN, A. L. & DURHAM, P. L. 1987 In vitro studies of vocal fold mucosa during isometric conditions. In *Laryngeal Function in Phonation and Respiration* (eds T. Baer, C. Sasaki & K. S. Harris). pp. 291–303. Boston: A College-Hill Press, Little, Brown and Company.

PELORSON, X., HIRSCHBERG, A., VAN HASSEL, R. R., WIJNANDS, A. P. J. & AUREGAN, Y. 1994a Theoretical and experimental study of quasisteady-flow separation within the glottis during phonation. Application to a modified two-mass model. *Journal of the Acoustical Society of America* **96,** 3416–3431.

PELORSON, X., HIRSCHBERG, A., AUREGAN, Y. & BAILLIET, H. 1994b Fluid dynamic aspects of voiced sound production: 1) A modified two-mass model. In *SMAC 93. Proceedings of the Stockholm Music Acoustics Conference*, July 28–August 1, 1993 (eds A. Friberg, J. Iwarsson, E. Jansson, & J. Sundberg), pp. 234–239. Royal Swedish Academy of Music.

PELORSON, X., HIRSCHBERG, A., WIJNANDS, A. P. J. & BAILET, H. 1995 Description of the flow through the vocal cords during phonation. *Acta Acustica* **3,** 191–202.

PETERKA, F. & SZÖLLÖS, O. 1999 Influence of the stop stiffness on impact oscillator dynamics. In *IUTAM Symposium on Unilateral Multibody Contacts* (eds F. Pfeiffer & Ch. Glocker), pp. 127–135. Netherlands: Kluwer Academic Publishers.

REUTER, R., HERZEL, H. & ORGLMEISTER, R. 1999 Simulations of vocal fold vibrations with an analog circuit. *International Journal of Bifurcation and Chaos* **9,** 1075–1088.
SIMERSKÁ, C. & HORÁČEK, J. 1996 Modelling of aeroelastic behaviour of a plate in channel. *Zeitschrift für angewandte Mathematik und Mechanik* **76,** 477–478.
STEINECKE, I. & HERZEL, H. 1995 Bifurcations in an asymmetric vocal fold model. *Journal of the Acoustical Society of America* **97,** 1874–1884.
ŠVEC, J., HORÁČEK, J., ŠRAM, F. & VESELÝ, J. 2000 Resonance properties of the vocal folds: in vivo laryngoscopic investigation of the externally excited laryngeal vibrations. *Journal of the Acoustical Society of America* **108,** 1397–1407.
TITZE, I. R. 1989 Physiologic and acoustic differences between male and female voices. *Journal of the Acoustical Society of America* **85,** 1699–1707.
TITZE, I. R. 1994 *Principles of Voice Production*. Englewood Cliffs, NJ: Prentice-Hall.
VERDOLINI-MARSTON, K., TITZE, I. R. & DRUKER, D. G. 1990 Changes in phonation threshold pressure with induced conditions of hydration. *Journal of Voice* **4,** 142–151.

APPENDIX A: EQUIVALENT MECHANICAL SYSTEM

The three masses m_1-m_3 of the equivalent mechanical system shown in Figure 3 were calculated from the following equations:

(a) equivalent mass of the system:

$$m = m_1 + m_2 + m_3; \tag{A1}$$

(b) equivalent static moment

$$-m_1(L/2) + m_2(L/2) = me; \tag{A2}$$

(c) equivalent moment of inertia:

$$m_1(L/2)^2 + m_2(L/2)^2 = I + me^2. \tag{A3}$$

The kinetic energy T of the system is

$$T = \frac{1}{2}m_1\dot{w}_1^2 + \frac{1}{2}m_2\dot{w}_2^2 + \frac{1}{2}m_3\left(\frac{\dot{w}_1 + \dot{w}_2}{2}\right)^2, \tag{A4}$$

and the potential energy is

$$\begin{aligned} V &= \frac{1}{2}\int_0^L cw^2(x,t)\,\mathrm{d}x \\ &= \frac{1}{2}\,c\int_0^L \left[w_1(t) + x\frac{w_2(t) - w_1(t)}{L}\right]^2 \mathrm{d}x \\ &= \frac{1}{6}\,k\,[w_1^2(t) + w_2^2(t) + w_1(t)w_2(t)], \end{aligned} \tag{A5}$$

where expressions (2) and (3) of the main text were used for $w(x,t)$ and the notation $k = cL$ was introduced for the coefficient of stiffness of the elastic foundation.

Substitution of T and V in the Lagrange equations:

$$\frac{\mathrm{d}}{\mathrm{d}t}\frac{\partial T}{\partial \dot{w}_j} - \frac{\partial T}{\partial w_j} + \frac{\partial V}{\partial w_j} = 0 \quad (j = 1, 2) \tag{A6}$$

gives the mass and stiffness matrices (6) in the equations of motion (5) of the equivalent mechanical system. The equivalent external (excitation) forces (4) were calculated from the

balance conditions:

$$F_1(t) + F_2(t) = h\int_0^L \tilde{p}(x,t)\,\mathrm{d}x, \quad F_2(t)L = h\int_0^L \tilde{p}(x,t)x\,\mathrm{d}x. \tag{A7}$$

APPENDIX B: LIST OF FUNCTIONS AND INTEGRALS INTRODUCED IN ANALYSIS

The functions and integrals introduced in expressions (22), (23) and (24) for aerodynamic forces are as follows:

$$I_1(x) = 1/2\int_0^x [y(y-L)/H(y)]\,\mathrm{d}y, \tag{B1}$$

$$I_2(x) = \int_0^x [y/H(y)]\,\mathrm{d}y, \quad I_3(x) = \int_0^x [1/H(y)]\,\mathrm{d}y, \tag{B2}$$

$$I_4(x) = \int_0^x [(y-L/2)\bar{U}_0(y)/H(y)]\,\mathrm{d}y, \quad I_5(x) = \int_0^x [\bar{U}_0(y)/H(y)]\,\mathrm{d}y, \tag{B3}$$

where

$$H(y) = H_0 - a(y); \tag{B4}$$

$$g_1(x) = I_4(x) + \bar{U}_0(x)(x/2)(x-L)/H(x), \quad g_2(x) = I_5(x) + \bar{U}_0(x)x/H(x), \tag{B5}$$

$$g_3(x) = \bar{U}_0(x)/H(x), \quad g_4(x) = (x-L/2)\bar{U}_0^2(x)/H(x), \quad g_5(x) = \bar{U}_0^2(x)/H(x); \tag{B6}$$

$$J_1 = \int_0^L I_1(x)(1-x/L)\,\mathrm{d}x, \quad J_2 = \int_0^L I_2(x)(1-x/L)\,\mathrm{d}x, \tag{B7}$$

$$J_3 = \int_0^L g_1(x)(1-x/L)\,\mathrm{d}x, \quad J_4 = \int_0^L g_2(x)(1-x/L)\,\mathrm{d}x, \tag{B8}$$

$$J_5 = \int_0^L g_4(x)(1-x/L)\,\mathrm{d}x, \quad J_6 = \int_0^L g_5(x)(1-x/L)\,\mathrm{d}x, \tag{B9}$$

$$J_7 = \int_0^L I_3(x)(1-x/L)\,\mathrm{d}x, \quad J_8 = \int_0^L g_3(x)(1-x/L)\,\mathrm{d}x, \tag{B10}$$

$$J_9 = \int_0^L (1-x/L)\,\mathrm{d}x = L/2, \quad J_{10} = \int_0^L I_1(x)(x/L)\,\mathrm{d}x, \tag{B11}$$

$$J_{11} = \int_0^L I_2(x)(x/L)\,\mathrm{d}x, \quad J_{12} = \int_0^L g_1(x)(x/L)\,\mathrm{d}x, \tag{B12}$$

$$J_{13} = \int_0^L g_2(x)(x/L)\,\mathrm{d}x, \quad J_{14} = \int_0^L g_4(x)(x/L)\,\mathrm{d}x, \tag{B13}$$

$$J_{15} = \int_0^L g_5(x)(x/L)\,\mathrm{d}x, \quad J_{16} = \int_0^L I_3(x)(x/L)\,\mathrm{d}x, \tag{B14}$$

$$J_{17} = \int_0^L g_3(x)(x/L)\,\mathrm{d}x, \quad J_{18} = \int_0^L (x/L)\,\mathrm{d}x = L/2. \tag{B15}$$

APPENDIX C: GOVERNING EQUATIONS FOR TUNING OF THE MECHANICAL SYSTEM

C.1. Calculation of the Elastic Foundation Stiffness k

The equation of motion (5) can be rewritten for the undamped mechanical system vibrating *in vacuo* as

$$\mathbf{M}\ddot{\mathbf{V}} + k\mathbf{K}_0\mathbf{V} = \mathbf{0}. \tag{C1}$$

where instead of the stiffness matrix $\mathbf{K}$ given by equation (6) the matrix $\mathbf{K}_0$, which does not depend on the coefficient of stiffness of the elastic foundation k, was introduced as

$$\mathbf{K} = k\mathbf{K}_0. \tag{C2}$$

Assuming the solution of the equation of motion in accordance with equation (42) as

$$\mathbf{V} = \mathbf{V}_0 \mathrm{e}^{st}, \tag{C3}$$

equation (C1) yields

$$(\mathbf{K} + \tilde{s}_j^2\mathbf{M})\tilde{\mathbf{V}}_{0j} = \mathbf{0}, \tag{C4}$$

where $\tilde{s}_j$ and $\tilde{\mathbf{V}}_{0j}$ $(j = 1, 2)$ are the eigenvalues and eigenvectors for the undamped mechanical system *in vacuo*. Substituting $\mathbf{K}$ from equation (C2) into the (C4) and dividing by k gives

$$(\mathbf{K}_0 + \tilde{s}_j^2/k\mathbf{M})\tilde{\mathbf{V}}_{0j} = \mathbf{0}. \tag{C5}$$

Denoting

$$\tilde{s}_{0j}^2 = \tilde{s}_j^2/k \tag{C6}$$

we can first solve the eigenvalue problem

$$(\mathbf{K}_0 + \tilde{s}_{0j}^2\mathbf{M})\tilde{\mathbf{V}}_{0j} = \mathbf{0}, \tag{C7}$$

where the matrices $\mathbf{K}_0$ and $\mathbf{M}$ are defined only by the geometry and material density of the vocal folds. Subsequently, the stiffness coefficient k is calculated from equation (C6) for $j = 1$, where the desired fundamental eigenfrequency (first eigenvalue $\tilde{s}_1$) is substituted.

Simultaneously, it follows from equations (C4)–(C6) that neither the ratio of the eigenfrequencies $\tilde{s}_1 : \tilde{s}_2$ nor the eigenvectors $\tilde{\mathbf{V}}_{01}$ and $\tilde{\mathbf{V}}_{02}$ depend on the stiffness k.

C.2. Calculation of the Damping Coefficients ε_1 and ε_2

According to equations (5) and (7), the equation of motion of the proportionally damped mechanical system vibrating *in vacuo* is given as

$$\mathbf{M}\ddot{\mathbf{V}} + \mathbf{B}\dot{\mathbf{V}} + \mathbf{K}\mathbf{V} = \mathbf{0}, \tag{C8}$$

where

$$\mathbf{B} = \varepsilon_1\mathbf{M} + \varepsilon_2\mathbf{K}. \tag{C9}$$

Substitution of $\mathbf{V}$ from equation (C3) into (C8) gives

$$[\mathbf{K} + s_j\mathbf{B} + s_j^2\mathbf{M}]\mathbf{V}_{0j} = \mathbf{0}, \tag{C10}$$

where s_j and $\mathbf{V}_{0j}$ are the eigenfunctions and eigenvectors for the damped mechanical system vibrating *in vacuo*. Left multiplication of equation (C10) by $\mathbf{V}_{0j}^{\mathrm{T}}$ and usage of equations (C4) and (C9) yields the following relationship between the eigenvalues of the damped (s_j) and undamped ($\tilde{s}_j$) mechanical systems:

$$-\tilde{s}_j^2 + s_j(\varepsilon_1 - \varepsilon_2\tilde{s}_j^2) + s_j^2 = 0. \tag{C11}$$

Introducing the notation

$$s_j = \mathfrak{Re}(s_j) + \mathrm{i}\mathfrak{Im}(s_j) \quad \text{and} \quad \tilde{s}_j = \mathrm{i}\mathfrak{Im}(\tilde{s}_j) \tag{C12}$$

equation (C11) can be divided into two equations for real and imaginary parts:

$$[\mathfrak{Im}^2(\tilde{s}_j)]^2 + \mathfrak{Re}(s_j)\{\varepsilon_1 + \varepsilon_2[\mathfrak{Im}(\tilde{s}_j)]^2\} + [\mathfrak{Re}(s_j)]^2 - [\mathfrak{Im}(s_j)]^2 = 0 \tag{C13}$$

$$\{\varepsilon_1 + \varepsilon_2[\mathfrak{Im}(\tilde{s}_j)]^2\} + 2\mathfrak{Re}(s_j) = 0. \tag{C14}$$

From the second equation rewritten for $j = 1, 2$ the damping coefficients ε_1 and ε_2 can be calculated

$$\varepsilon_1 = 2\frac{\mathfrak{Re}(s_2)[\mathfrak{Im}(\tilde{s}_1)]^2 - \mathfrak{Re}(s_1)[\mathfrak{Im}(\tilde{s}_2)]^2}{[\mathfrak{Im}(\tilde{s}_2)]^2 - [\mathfrak{Im}(\tilde{s}_1)]^2}, \quad \varepsilon_2 = 2\frac{\mathfrak{Re}(s_2) - \mathfrak{Re}(s_1)}{[\mathfrak{Im}(\tilde{s}_1)]^2 - [\mathfrak{Im}(\tilde{s}_2)]^2}. \tag{C15, C16}$$

Assuming that the eigenfrequencies of the damped and undamped systems are approximately the same, i.e., $\mathfrak{Im}(s_i) \approx \mathfrak{Im}(\tilde{s}_i)$, and introducing the eigenfrequencies $f_j = s_j/2\pi$ and 3 dB half-power bandwidths $\Delta f_j = -2\mathfrak{Re}(f_j) = -\mathfrak{Re}(s_j)/\pi$, formulas (C15) and (C16) can be finally rewritten as equations (46), which were used for calculation of the damping coefficients ε_1 and ε_2 according to the experimental data.